Available online at www.sciencedirect.com
SCIENCE DIRECT®
ELSEVIER
Nuclear Instruments and Methods in Physics Research A 543 (2005) 463–482
NUCLEAR INSTRUMENTS & METHODS IN PHYSICS RESEARCH Section A
www.elsevier.com/locate/nima

The effect of highly ionising particles on the CMS silicon strip tracker

W. Adam[a], T. Bergauer[a], M. Friedl[a], R. Fruehwirth[a], J. Hrubec[a], M. Krammer[a], M. Pernicka[a], W. Waltenberger[a], W. Beaumont[b], E. de Langhe[b], E. de Wolf[b], M. Tasevsky[b], O. Bouhali[c], B. Clerbaux[c], G. de Lentdecker[c], J.-P. Dewulf[c], L. Neuckermans[c], C. Vander-Velde[c], P. Vanlaer[c], J. Wickens[c], J. D'Hondt[d], R. Goorens[d], J. Heyninck[d], S. Lowette[d], S. Tavernier[d], L. Van Lancker[d], C. Yu[d], S. Assouak[e], J.-L. Bonnet[e], G. Bruno[e], B. De-Callatay[e], J. De-Favereau-de-Jeneret[e], C. Delaere[e], S. De-Visscher[e], D. Favart[e], G. Gregoire[e], Th. Keutgen[e], G. Leibenguth[e], V. Lemaitre[e], D. Michotte[e], O. Militaru[e], A. Ninane[e], S. Ovyn[e], K. Piotrzkowski[e], V. Roberfroid[e], X. Rouby[e], O. Van-der-Aa[e], M. Vander-Donckt[e], I. Boulogne[f], E. Daubie[f], F. Defontaines[f], P. Herquet[f], S. Czellar[g], J. Härkönen[g], V. Karimäki[g], H. Katajisto[g], T. Linden[g], P. Luukka[g], T. Lampen[g], T. Mäenpää[g], E. Tuominen[g], J. Tuominiemi[g], T. Tuuva[h], M. Ageron[i], E. Chabanat[i], D. Contardo[i], N. Estre[i], R. Haroutunian[i], N. Lumb[i], L. Mirabito[i], S. Perries[i], B. Trocme[i], R. Blaes[j], F. Charles[j], F. Drouhin[j], J.P. Ernenwein[j], J.C. Fontaine[j], J.D. Berst[k], J.M. Brom[k], F. Didierjean[k], U. Goerlach[k], L. Gross[k], P. Juillot[k], A. Lounis[k], C. Maazouzi[k], C. Olivetto[k], R. Strub[k], P. Vanhove[k], D. Vintache[k], R. Adolphi[l], R. Brauer[l], W. Braunschweig[l], H. Esser[l], L. Feld[l], A. Heister[l], W. Karpinski[l], K. Klein[l], S. König[l], C. Kukulies[l], J. Olzem[l], A. Ostaptchouk[l], D. Pandoulas[l], G. Pierschel[l], F. Raupach[l], S. Schael[l], A. Schultz von Dratzig[l], G. Schwering[l], R. Siedling[l], M. Thomas[l], M. Wlochal[l], F. Beissel[m], K.-D. Boffin[m], M. Duda[m], A. Flossdorf[m], G. Flugge[m], T. Franke[m], K. Hangarter[m], B. Hegner[m], Th. Hermanns[m], S. Kasselmann[m], Th. Kress[m], A. Linn[m], J. Mnich[m], A. Nowack[m], M. Poettgens[m], O. Pooth[m], B. Reinhold[m], M. Bleyl[n], U. Holm[n], R. Klanner[n], U. Pein[n],

*Corresponding authors. CERN, Mailbox E22210, 40-4-B32, Geneva 23 CH-1211, Switzerland. Tel.: +41 22 767 1666; fax: +41 22 767 8940.

E-mail addresses: Simone.Paoletti@cern.ch (S. Paoletti), robert.bainbridge@cern.ch (R. Bainbridge).

0168-9002/$ - see front matter
doi:10.1016/j.nima.2004.11.049

P. Schleper[n], N. Schirm[n], G. Steinbrück[n], M. Stoye[n], S. Tesch[n], R. van Staa[n], K. Wick[n], B. Atz[o], T. Barvich[o], P. Blum[o], W. de Boer[o], F. Boegelspacher[o], G. Dirkes[o], M. Fahrer[o], J. Fernandez[o], M. Frey[o], A. Furgeri[o], E. Grigoriev[o], F. Hartmann[o], S. Heier[o], T. Muller[o], T. Ortega-Gomez[o], H.-J. Simonis[o], P. Steck[o], A. Theel[o], T. Weiler[o], V. Zhukov[o], D. Creanza[p], N. De Filippis[p], M. de Palma[p], G. De Robertis[p], L. Fiore[p], D. Giordano[p], G. Maggi[p], M. Mennea[p], S. My[p], V. Radicci[p], G. Selvaggi[p], L. Silvestris[p], P. Tempesta[p], G. Zito[p], S. Albergo[q], V. Bellini[q], M. Chiorboli[q], S. Costa[q], R. Potenza[q], C. Sutera[q], A. Tricomi[q], C. Tuvè[q], A. Bocci[r], V. Ciulli[r], C. Civinini[r], R. D'Alessandro[r], E. Focardi[r], G. Landi[r], A. Macchiolo[r], N. Magini[r], S. Mersi[r], C. Marchettini[r], M. Meschini[r], S. Paoletti[r,*], G. Parrini[r], R. Ranieri[r], M. Sani[r], N. Bacchetta[s], D. Bisello[s], A. Candelori[s], T. Dorigo[s], P. Giubilato[s], A. Kaminsky[s], M. Loreti[s], M. Nigro[s], A. Paccagnella[s], R. Rando[s], M.M. Angarano[t], E. Babucci[t], D. Benedetti[t], M. Biasini[t], G.M. Bilei[t], M.T. Brunetti[t], B. Checcucci[t], N. Dinu[t], L. Fanò[t], M. Giorgi[t], P. Lariccia[t], G. Mantovani[t], V. Postolache[t], M. Puscalau[t], D. Ricci[t], R. Santinelli[t], A. Santocchia[t], L. Servoli[t], C. Zucchetti[t], P. Azzurri[u], G. Bagliesi[u], A. Basti[u], J. Bernardini[u], T. Boccali[u], L. Borrello[u], F. Bosi[u], R. Castaldi[u], M. D'Alfonso[u], R. Dell'Orso[u], S. Dutta[u], L. Foa[u], S. Gennai[u], A. Giammanco[u], A. Giassi[u], T. Lomtadze[u], B. Mangano[u], A. Messineo[u], A. Moggi[u], F. Palla[u], F. Palmonari[u], F. Raffaelli[u], A. Rizzi[u], D. Rizzi[u], G. Segneri[u], D. Sentenac[u], G. Sguazzoni[u], P. Spagnolo[u], G. Tonelli[u], P.G. Verdini[u], C. Biino[v], M. Costa[v], N. Demaria[v], G. Favro[v], P. Trapani[v], C. Peroni[v], A. Romero[v], E. Migliore[v], D. Abbaneo[w], F. Ahmed[w], P. Bartalini[w], N. Bernardino-Rodriguez[w], H. Breuker[w], O. Buchmuller[w], E. Carrone[w], A. Cattai[w], R. Chierici[w], S. Cucciarelli[w], A. Dierlamm[w], M. Eppard[w], A. Frey[w], K. Gill[w], R. Grabit[w], A. Honma[w], M. Huhtinen[w], G. Magazzu[w], M. Mannelli[w], A. Marchioro[w], A. Onnela[w], B. Perea-Solano[w], P. Petagna[w], H. Postema[w], M. Risoldi[w], G. Rolandi[w], P. Siegrist[w], I. Troska[w], A. Tsirou[w], F. Vasey[w], M. Weber[w], B. Wittmer[w], W. Bertl[x], K. Gabathuler[x], R. Horisberger[x], H.-Ch. Kästli[x], D. Kotlinski[x], A. MacPherson[x], T. Rohe[x], K. Freudenreich[y], W. Lustermann[y], F. Pauss[y], R. Eichler[z], W. Erdmann[z], C. Grab[z], A. Schoning[z], C. Amsler[aa], V. Chiochia[aa], A. Dorokhov[aa], C. Hörmann[aa], H. Pruys[aa], K. Prokofiev[aa], C. Regenfus[aa], P. Robmann[aa], T. Speer[aa], K.W. Bell[ab], J. Coughlan[ab], M. French[ab], R. Halsall[ab], L. Jones[ab], M. Pearson[ab], G. Rogers[ab], I. Tomalin[ab], R. Bainbridge[ac,*], P. Barrillon[ac], D. Colling[ac], S. Dris[ac], C. Foudas[ac], J. Fulcher[ac], G. Hall[ac], G. Iles[ac], J. Jones[ac], J. Leaver[ac], B.C. Macevoy[ac], M. Noy[ac], D.M. Raymond[ac], M. Takahashi[ac], O. Zorba[ac], B. Barnett[ad], C.-Y. Chien[ad], D.W. Kim[ad], G. Liang[ad], M. Swartz[ad], M. Atac[ae],

M. Demarteau[ae], U. Joshi[ae], S. Kwan[ae], L. Spiegel[ae], S. Tkaczyk[ae], C.E. Gerber[af], E. Shabalina[af], T. Ten[af], R. Lander[ag], D. Pellett[ag], B. Gobbi[ah], M. Kubantsev[ah], S. Malik[ah], R. Tilden[ah], P. Baringer[ai], A. Bean[ai], L. Christofek[ai], D. Coppage[ai], T.A. Bolton[aj], R. Demina[aj], W.E. Kahl[aj], A. Khanov[aj], S. Korjenevski[aj], N. Pukhaeva[aj], N.W. Reay[aj], F. Rizatdinova[aj], R.A. Sidwell[aj], N.R. Stanton[aj], L. Cremaldi[ak], D. Sanders[ak], E. Bartz[al], J. Doroshenko[al], T. Koeth[al], L. Perera[al], S. Schnetzer[al], R. Stone[al], S. Worm[al], P. Gartung[am], G.G. Hanson[am], G.Y. Jeng[am], G. Páztor[am,1], R. Eusebi[an], E. Halkiadakis[an], A. Hocker[an], P. Tipton[an], A. Affolder[ao], C. Campagnari[ao], D. Hale[ao], J. Incandela[ao], S. Kyre[ao], J. Lamb[ao], R. Taylor[ao], D. White[ao], G. Bolla[ap], D. Bortoletto[ap], A. Garfinkel[ap], C. Rott[ap], A. Roy[ap]

[a]*Institut für Hochenergiephysik der Öesterreichischen Akademie der Wissenschaften, HEPHY, Vienna, Austria*
[b]*Universiteit Antwerpen, Belgium*
[c]*Brussels-ULB, Belgium*
[d]*Brussels-VUB, Belgium*
[e]*Louvain, Belgium*
[f]*Mons, Belgium*
[g]*University of Helsinki-HIP, Finland*
[h]*Lappeenranta University of Technology, Finland*
[i]*Lyon, France*
[j]*Universite de Haute Alsace, Mulhouse, France*
[k]*Institut de Recherches Subatomiques, Strasbourg, France*
[l]*I. Physikalisches Institut, RWTH, Aachen, Germany*
[m]*III. Physikalisches Institut, RWTH, Aachen, Germany*
[n]*University of Hamburg, Germany*
[o]*Karlsruhe-IEKP, Germany*
[p]*INFN and Dipartimento Interateneo di Fisica, Bari, Italy*
[q]*INFN and University of Catania, Italy*
[r]*INFN and University of Firenze, Firenze, Italy*
[s]*INFN and University of Padova, Italy*
[t]*INFN and University of Perugia, Italy*
[u]*INFN and University of Pisa and Scuola Normale Superiore di Pisa, Italy*
[v]*INFN and University of Torino, Italy*
[w]*European Organization for Nuclear Research (CERN), Geneva, Switzerland*
[x]*Paul Scherrer Institut, PSI, Villigen, Switzerland*
[y]*Eidgenössische Technische Hochschule, IPP-LHP, Zürich, Switzerland*
[z]*Eidgenössische Technische Hochschule, IPP-LPP, Zürich, Switzerland*
[aa]*University of Zürich, Switzerland*
[ab]*Rutherford Appleton Laboratory, Chilton, Didcot, UK*
[ac]*Imperial College London, UK*
[ad]*Johns Hopkins University, Baltimore, MD, USA*
[ae]*Fermilab, Batavia, IL, USA*
[af]*University of Illinois, Chicago, IL, USA*
[ag]*University of California Davis, Davis, CA, USA*
[ah]*Northwestern University, Evanston, IL, USA*
[ai]*University of Kansas, Lawrence, KS, USA*
[aj]*Kansas State University, Manhattan, KS, USA*
[ak]*University of Mississippi, USA*
[al]*Rutgers University, Piscataway, NJ, USA*

[1]G. Páztor is also at the Research Institute for Particle and Nuclear Physics, Budapest, Hungary.

[am] University of California, Riverside, USA
[an] University of Rochester, Rochester, NY, USA
[ao] University of California, Santa Barbara, CA, USA
[ap] Purdue University, West Lafayette, IN, USA

Received 12 November 2004; accepted 27 November 2004
The CMS Tracker Collaboration
Available online 22 January 2005

Abstract

Inelastic nuclear collisions of hadrons incident on silicon sensors can generate secondary highly ionising particles (HIPs) and deposit as much energy within the sensor bulk as several hundred minimum ionising particles. The large signals generated by these 'HIP events' can momentarily saturate the APV25 front-end readout chip for the silicon strip tracker (SST) sub-detector of the compact muon solenoid (CMS) experiment, resulting in deadtime in the detector readout system. This paper presents studies of this phenomenon through simulation, laboratory measurements and dedicated beam tests. A proposed change to a front-end component to reduce the APV25 sensitivity to HIP events is also examined. The results are used to infer the expected effect on the performance of the CMS SST at the future large hadron collider. The induced inefficiencies are at the percent level and will have a negligible effect on the physics performance of the SST.

PACS: 07.50.−e; 07.89.+b; 29.40.Gx; 85.40.−e

Keywords: CMS; Silicon strip tracker; APV25; Highly ionising particles

1. Introduction

Inelastic interactions between hadrons and the nuclei of silicon sensors can heavily ionise the bulk through the production of highly ionising particles (HIPs), such as recoiling nuclei and nuclear fragments. Although these 'HIP events' are rare, $O(10^{-3})$ per incident hadron, they are responsible for generating energy depositions up to three orders of magnitude greater than those typically released by a minimum ionising particle (MIP). HIP events were first observed to saturate the APV25 front-end chip and introduce significant deadtime into the detector readout system during a beam test at the CERN X5 beamline [1]. The APV25 [2] is the 128-channel analogue readout chip for the silicon strip tracker (SST) [3] of the compact muon solenoid (CMS) detector [4].

HIP events are easily identifiable due to the characteristic response of the APV25 chip. A typical HIP event is shown in Fig. 1(a), which plots the pulse height data (after subtraction of static 'pedestal' values unique to each channel) read out from the 512 channels of an affected sensor. Large signals are observed for the few channels (of APV#2) on which the HIP-induced energy deposition is collected and, crucially, the pulse height data of all remaining channels of the affected APV25 chip are depressed. Adjacent chips are unaffected. The observed shifts in the data are interpreted by the analysis software as a negative common mode (CM) level, hence HIP events are responsible for the long tail in the CM distribution shown in Fig. 1(b). As the pulse height data cannot fall below a certain level due to limits on the voltages internal to the chip, a peak is observed in the distribution at a minimum CM level.

This paper describes the various studies undertaken in order to understand and quantify the effect of HIP events on the APV25 and the SST readout system. Section 2 describes a simulation of nuclear interactions in silicon sensors that provides energy deposition probability spectra. Section 3 provides a qualitative explanation of how the APV25 chip is affected by HIP events and identifies a method to moderate the effect, which

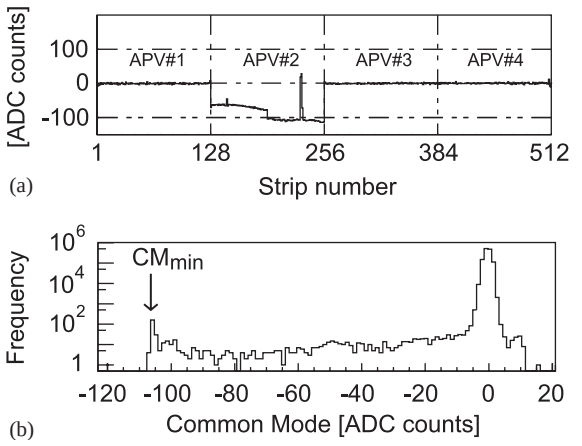

Fig. 1. (a) Pulse height data read out from 512 channels of a sensor plane affected by a HIP event. (b) Distribution of CM levels for an individual APV25 chip. The tail is a consequence of the APV25 behaviour in response to HIP events.

is examined experimentally through the laboratory studies described in Section 4. All subsequent sections are concerned with a dedicated beam test performed at the Paul Scherrer Institut (PSI) and further complementary beam test studies performed using the CERN X5 beamline. The experimental set-ups are described in Section 5. Analyses of the beam test data, fully described in Ref. [5], are then reported, which provide measurements of the 'HIP event' probability (Section 6), a study of the APV25 recovery (Section 7) and measurements of the induced inefficiencies (Section 8). Finally, Section 9 examines the implications of HIP events for the expected performance of the SST.

2. Simulations of nuclear interactions in silicon sensors

Simulations of nuclear interactions in silicon sensors [6] provide probability spectra describing the magnitude and spatial extent of HIP-induced energy depositions. This information cannot be inferred from the APV25 output data due to signal truncation (at a level equivalent to 8 MIPs in 300 μm of silicon) and inter-strip capacitive coupling within the sensor. The simulations are essentially identical to those used to estimate single event upset (SEU) rates in CMS [7]. The principal difference is that the SEU simulations are primarily concerned with heavy nuclear fragments that generate highly localised energy depositions within a small sensitive volume of the order μm^3, whereas for the HIP simulations all interaction products have to be considered.

The simulations reveal that the energy spectra of heavy fragments ($Z \gg 1$) produced in silicon are largely insensitive to the incident particle energy and do not extend beyond ~10 MeV. The maximum rate of energy loss for heavy ions, such as silicon and magnesium, in silicon is of the order $MeV\,\mu m^{-1}$, hence heavy nuclear fragments are typically limited to ranges of $<100\,\mu m$ [7]. Light particles generated in inelastic collisions, such as pions and protons, have energy spectra that scale with the energy of the incident particle, a maximum energy loss rate of the order $100\,keV\,\mu m^{-1}$ (at 100 keV) and generally long ranges in silicon. Since the sensor dimensions define a large 'sensitive volume', these light particles also contribute significantly to the total energy deposition. The treatment of elastic and inelastic nuclear interactions and the transport (under zero magnetic field) of the interaction products and their energy loss mechanisms are discussed in Ref. [6] (and references therein).

Fig. 2 plots the simulated energy deposition differential probability spectra for 200 MeV pions normally incident on a 500-μm-thick tracker outer barrel (TOB) sensor; both the elastic and total spectra are shown. Energy depositions of up to ~100 MeV are predicted, with only inelastic events generating depositions greater than a few MeV. Since heavy fragments can only deposit up to ~10 MeV, events with the highest depositions always involve several particles. The apparent bumps in the elastic spectrum result from the diffractive structure of the elastic angular distribution.

Fig. 3 plots the energy deposition integral probability curves, per incident particle, for tracker inner barrel (TIB) and TOB sensors illuminated by hadrons with energy spectra and fluxes corresponding to that expected in the TIB and TOB regions. The hadron energy spectra, all of

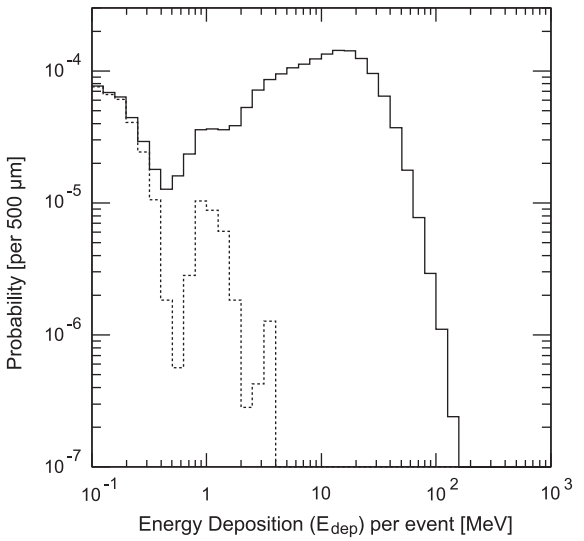

Fig. 2. Energy deposition differential probability spectra for both elastic and inelastic collisions (solid line) and elastic collisions only (dashed line) with 200 MeV pions normally incident on a 500-μm-thick TOB sensor [6].

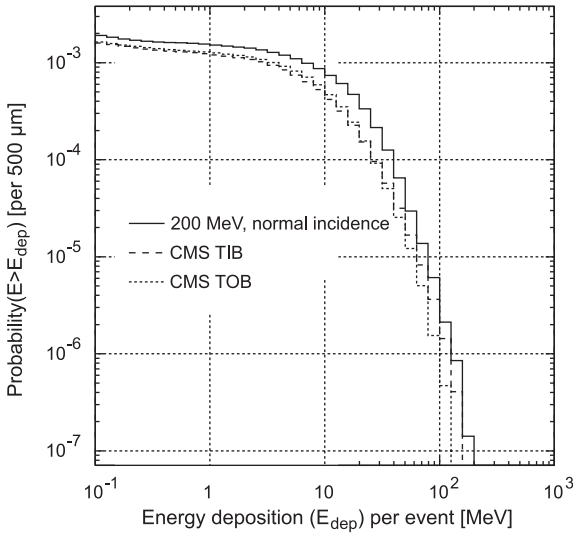

Fig. 3. Energy deposition integral probability per incident particle, for: hadrons incident on TIB and TOB sensors with energy spectra and fluxes corresponding to those expected in the TIB and TOB regions; 200 MeV pions normally incident on a TOB sensor. All probabilities are normalised to a 500 μm path length in silicon [6].

which peak at energies of ~100 MeV, can be found in Appendix A of Ref. [3]. The hadron fluxes expected at the innermost and outermost SST sensor planes (found in the TIB and TOB regions, respectively) are summarised in Table 1. An isotropic angular distribution was assumed so as to reflect the range of particle incidence angles expected in the SST environment.

The interaction probability is normalised to reflect a 500 μm path length in silicon by weighting each simulated interaction by the factor $500\,\mu m/d$, where d (μm) is the interpolated path length of the incident hadron in the sensor. This normalisation permits a comparison of the TIB and TOB integral probability curves with the curve for 200 MeV pions normally incident on a 500-μm-thick TOB sensor, also shown in Fig. 3. The integral probability curves are relatively flat up to ~10 MeV, but fall away quickly beyond this energy. However, depositions of up to ~200 MeV are observed, which corresponds to ~1400 MIPs in 500 μm of silicon.[2] The reduction in the TIB and TOB integral probabilities with respect to those for 200 MeV pions is due to the lower (average) cross-section and the samples containing hadrons with energies <200 MeV. The effect of the isotropic angular distribution on the induced energy deposition, due to the increased path length of light secondaries in the sensor, is negligible as no significant enhancement of the tail is observed for the TIB and TOB curves.

Table 1
Hadron fluxes ($10^6\,cm^{-2}\,s^{-1}$) for the innermost and outermost sensor layers of the CMS SST (barrel region) at the LHC pp luminosity of $10^{34}\,s^{-1}$

Radius (cm)	22	115
Pion	2.06 ± 0.03	0.030 ± 0.002
Proton	0.203 ± 0.007	0.008 ± 0.001
Kaon	0.183 ± 0.006	0.005 ± 0.001
Neutron >20 MeV	0.330 ± 0.010	0.059 ± 0.001
Hadrons >20 MeV	2.77 ± 0.03	0.102 ± 0.002

The quoted errors reflect only the simulation statistics [6].

[2]This conversion assumes a MIP release of $40,000\,e/h$ pairs and deposits 144 keV in 500 μm of silicon.

3. Explanation of the APV25 behaviour

The simulations described above predict that the most probable energy deposition generated by inelastic nuclear interactions in silicon sensors is ~10 MeV. Energy depositions of this magnitude saturate the front-end amplifying stages of the collecting channels and render them insensitive to further signals for several hundred nanoseconds. Crucially, all remaining channels of the APV25 are also affected. This is a consequence of crosstalk on the chip, which is exacerbated by the biasing scheme used to power the front-end inverter and shaper stages.[3] Power for the inverter and shaper stages of the 128 channels is derived from a common +2.5 V supply rail via an external 'inverter' resistor, R_{inv} (nominally 100 Ω).

A beneficial feature of this biasing scheme is the effective removal of any external CM component to the pulse height data, resulting in a very stable baseline under normal operating conditions [9]. This stable behaviour is evidenced in Fig. 1(b), which shows a strong narrow peak at zero in the distribution of CM levels. However, large signals ($\gg$MIP) at the inverter (or shaper) input nodes of one or more channels will drive down the inverter (or shaper) outputs of all other channels of the affected chip. This feature is observed in the APV25 data as a shift (of opposite polarity to signal) in the analogue levels of all channels. Hence, a sufficiently large signal can temporarily render all 128 channels insensitive to further signals, resulting in deadtime. These shifts in the data are interpreted as non-zero CM levels and are responsible for the long tail at negative CM levels shown in Fig. 1(b). Frequently, the depressed pulse height data are non-uniform, resulting in sloping baselines.

The behaviour of the APV25 front-end amplifying stages under the influence of large signals has been simulated using the HSPICE package [10]. Even though the study was required to simulate circuit components that are operating well outside their design specifications, the predicted deadtimes closely match observations made in the laboratory and beam tests. Importantly, the simulation predicted that a reduced inverter resistor value would increase the available power to the inverter and shaper stages and consequently moderate the influence of HIP events on the APV25 chip. The simulation predicted smaller shifts in the pulse height data, shorter periods of insensitivity (deadtime) and an increase in the threshold energy deposition required for deadtime to be observed.

[3]The switchable inverter stage allows readout of sensors with either n- or p-type bulk (and therefore signals of either polarity) and ensures the full use of the dynamic range of the shaper stage, which provides 50 ns CR–RC filtering [8].

4. Laboratory studies of HIP events

The simulation studies described in Section 2 predict large fluctuations in the magnitude (and spatial extent) of HIP-induced energy depositions, hence an accurate simulation of the effect in the laboratory is difficult to achieve. Nevertheless, laboratory studies can provide useful and important information; for example, the APV25 behaviour can be studied over a longer time period and in more detail than possible in the beam test environment and the observed deadtimes can be related to known input signals. Two independent studies, described below, provide systematic measurements of deadtimes observed in the APV25 chip for a range of large signals collected on various numbers of channels. The primary aim of these studies is to assess the expected improvements in the chip recovery with a reduced inverter resistor value. Additionally, the studies quantify the deadtime dependence on the magnitude of the simulated energy depositions and the effect of the different operational modes of the chip on the observed deadtimes.

HIP events are simulated either by injecting charge directly into channels of the APV25 via the bond pads on the front-end of the chip [1] or by pulsing a 1060 nm laser to illuminate a TOB sensor instrumented with APV25 chips [11]. For the former case, no sensor is used and neighbouring channels are coupled to the injected charge via a capacitor network to simulate the inter-strip capacitive coupling expected from a sensor. Both methods investigate the APV25 behaviour following a HIP event by generating MIP-like signals on

a channel different from those collecting the charge released by the simulated HIP event and scanning the delay time between the two signals. The APV25 is triggered to coincide with the peaking time of the MIP signal and its response is reconstructed as a function of time.

4.1. Simulating HIP events through charge injection

The magnitude of the simulated HIP event is accurate to ±5% (attributable to the non-negligible tolerance of the charge injection capacitors). The APV25 chip is operated in deconvolution and inverting modes. The temporal response of the APV25 to a 3-MIP signal is reconstructed for various charge injections that simulate HIP energy depositions in the range 10–100 MeV, as illustrated in Fig. 4. The traces clearly show that the magnitude of the 3-MIP signal is fully depressed for sufficiently large energy depositions; the period for which the signal is fully depressed is defined as the deadtime induced by the HIP event. Fig. 5 plots the measured deadtime as a function of energy deposition, with charge injected on two adjacent channels (with neighbouring channels coupled to the signal via the capacitor network) and for two different resistor values.

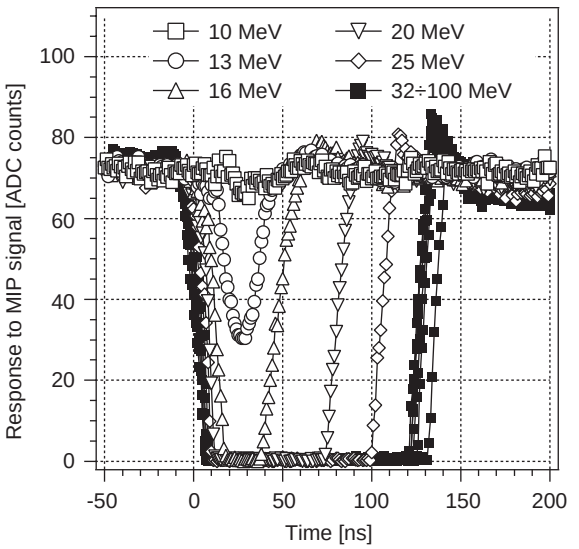

Fig. 4. Temporal response of the APV25 to a 3-MIP signal for simulated HIP energy depositions of 10–25 MeV (open symbols) and 32–100 MeV (closed symbols). The results shown are for a resistor value of 100 Ω and charge injection on a single channel.

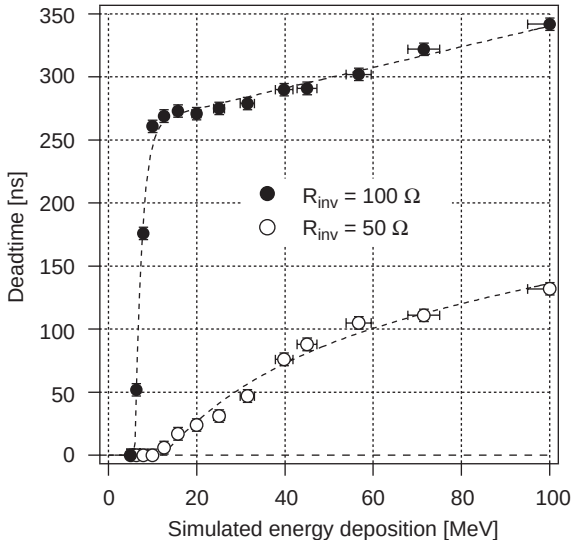

Fig. 5. Deadtime as a function of HIP event magnitude (with charge injected on two adjacent channels) for modules equipped with inverter resistors of 100 Ω (closed markers) and 50 Ω (open markers).

The deadtime dependency on the energy deposition is parameterised, as illustrated by the best fits (dashed lines) in Fig. 5. The dependency is characterised by a threshold deposition required for deadtime to be observed, E_{thr}, followed by an initial exponential dependence and a subsequent linear rise; T_{max} is the deadtime observed for an energy deposition of 100 MeV. Both E_{thr} and T_{max} are strongly dependent on the inverter resistor value and the number of channels on which the charge is injected; this dependence is shown in Table 2. With fewer collecting channels or a lower resistor value, an improvement is observed: E_{thr} increases and T_{max} decreases.

4.2. Simulating HIP events with a laser

Using a fixed laser pulse duration (3 ns), the ionisation charge released in the sensor is controlled by varying the laser bias voltage. The resulting energy deposition is calibrated by

Table 2
Threshold energy deposition, E_{thr}, and maximum observable deadtime, T_{max}, for various inverter resistor values, R_{inv}, and charge-collecting channels, N_{chan} (with or without capacitive coupling)

N_{chan}	R_{inv} (Ω)	E_{thr} (MeV)	T_{max} (ns)
1 (+CC)	100	11.9 ± 0.3	140
2 (+CC)	100	6.0 ± 0.1	340
7	100	9.0 ± 0.3	1500
1 (+CC)	50	18.9 ± 0.1	110
2 (+CC)	50	12.3 ± 1.4	130

measuring changes in the sensor bias ('dark') current, ΔI (nA), when the laser is pulsed at a high frequency f (kHz). The released energy is given by E_{dep} (eV) $= (3.6 \times \Delta I)/(e \times f)$, where the factor 3.6 (eV) represents the ionisation energy in silicon and e (C) is the electron charge. The calibration is accurate to ±10% and depositions in the range 15–45 MeV are achieved. A second 1060 nm laser is pulsed to induce a signal equivalent to 1 MIP (500 μm silicon) within the sensor of the TOB module. The laser light is focused on a region between two adjacent strips and their aluminium layering (resulting in the laser-generated charge being collected on 1–2 channels). The two light spots are separated by approximately 100 strips (18.3 mm) and incident upon a sensor region instrumented by the same APV25 chip. The APV25 chip is operated in both peak and deconvolution modes and inverting and non-inverting modes.

Figs. 6(a) and (b) compare, for TOB modules equipped with 100 and 50 Ω inverter resistors, respectively, the temporal evolution of the APV25 baseline (circular markers) and signal response (triangular markers) following a simulated HIP event of magnitude 25 MeV. As before, the deadtime is defined as the period for which no signal is observed. Efficient cluster reconstruction (and therefore hit recognition) is assumed when $(S/N)/(S/N)_{ref} \geqslant 0.25$, where $(S/N)_{ref}$ is the signal-to-noise ratio observed under normal operating conditions [11]. Therefore, in addition to deadtime, the 'recovery time' is defined as the period for which the MIP signal is sufficiently depressed such that cluster reconstruction is inefficient.

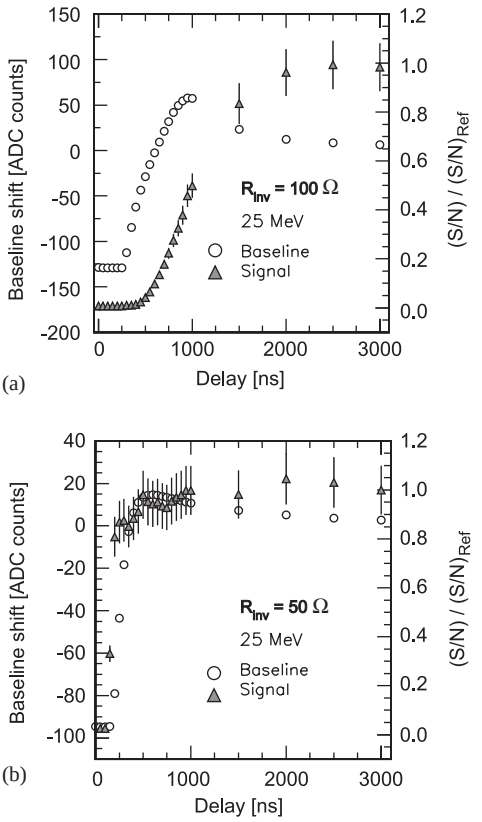

Fig. 6. Time evolution of the APV25 recovery, expressed in terms of CM level (circles) and signal-to-noise (S/N) value (triangles). The recoveries are shown for chips equipped with a resistor value of (a) 100 Ω and (b) 50 Ω and a simulated HIP energy deposition of 25 MeV.

Table 3 summarises the measured deadtimes and recovery times observed for various HIP energies and the two inverter resistor values, with the APV25 operated in its standard configuration of deconvolution and inverting modes. Both the deadtime and recovery time of the chip are significantly reduced for the 50 Ω case. Similar measurements are also performed with the chip operated in peak and/or non-inverting modes, which revealed significant reductions in the observed deadtimes and recovery times; the maximum observed recovery time when operating in non-inverting mode is < 100 ns.

Table 3
Deadtimes and recovery times for various HIP-induced energy depositions with resistor values of 100 Ω or 50 Ω (50 Ω results in brackets)

E_{dep} (MeV)	T_{dead} (ns)	T_{recov} (ns)
15 (15)	100 (100)	200 (100)
25 (23)	500 (150)	800 (150)
35 (28)	600 (250)	700 (250)
45 (31)	700 (300)	800 (300)

The APV25 is operated in deconvolution and inverting modes. Note that measurements are performed at different energies for the two resistor values.

4.3. Comparison and experimental uncertainties

The laser-based measurements with the APV25 chip operating in deconvolution and inverting modes can be compared with those obtained through direct charge injection. The deadtime observed with the 100 Ω (50 Ω) inverter resistor and a laser-generated deposition of 45 MeV (31 MeV) is 700 ns (300 ns), which compares with the corresponding measurements of 124 ns (76 ns) obtained with direct charge injection on a single channel and 291 ns (47 ns) on two channels. A charge injection equivalent to an energy deposition of 45 MeV and shared between seven APV25 channels (without capacitive coupling) induces a deadtime of 1250 ns.

The discrepancies in the measured deadtimes are not unexpected, given the different methods employed to simulate HIP events and the sensitivity of the APV25 chip to the spatial distribution of the collected signal. Although the first method attempts to simulate the inter-strip capacitive coupling of a sensor using a capacitive network, it cannot exactly reproduce the spatial distribution of the collected signal or account for further coupling paths external to the APV25 chip such as, for example, on the pitch adapter connecting the sensor to the APV25 chip. The laser-based measurements are performed using a sensor, but again the highly localised energy depositions typical of a HIP event cannot be exactly reproduced using a laser and the spatial extent of the generated energy deposition cannot be precisely known due to uncertainties associated with the focusing of the laser light and internal reflections within the sensor. As a consequence of these uncertainties, the beam test measurements described in the following sections are considered definitive when extrapolating the effect to the expected CMS environment, and are used to predict the rates and total inefficiencies.

5. Beam test studies of HIP events

5.1. Experimental set-up for the PSI beam test

The PSI πM1 beamline provides a continuous 50 MHz bunched beam of pions (of both charges) at a maximum flux of 0.8 MHz cm^{-2} (comparable to that expected at the innermost detector layer of the SST during high-intensity LHC operation). The beam momentum was tuned to 300 MeV/c, which corresponds to the most probable pion momentum generated by minimum bias events in the SST [3] and the enhanced πSi interaction cross-section at the $\Delta(1232)$ resonance. Four categories of run conditions are considered: 'low' and 'high' ($\times 2$) intensity π^- beams and a 'medium' intensity π^+ beam with the APV25 operating in either inverting or non-inverting mode. The beamline also delivers 300 MeV/c protons.

The tracking unit comprised 12 new detector modules[4] simultaneously exposed to the beam [5]; three modules were of type TIB, three Tracker End-Cap (TEC) and six TOB. The modules were equipped with inverter resistors of either the nominal (100 Ω) or reduced (50 Ω) value. The APV25 chips were operated in peak mode throughout the beam test. The control and data acquisition systems were PC-based, with the analogue data transferred electrically to ADC cards housed in local PCs.

Triggers were defined by coincident signals from two photo-multipliers viewing the same scintillation counter upstream of the tracking unit. An additional downstream counter was used in coincidence or anti-coincidence for HIP event studies

[4] A detector module comprises a sensor, the APV25 readout chips, other ancillary chips and the support and cooling structures.

or as a proton veto when using the π^+ beam. A PC-based sequencer card limited triggers to bunch crossings when both the 50 MHz beam clock and the 40 MHz clock used by the readout system were synchronous. Special trigger combinations were used to collect useful data samples for analysis. A trigger pre-filter was imposed throughout the beam test comprising a particle veto of duration 300 ns to remove the 'pile-up' of HIP events in bunch crossings prior to each trigger. A 'single trigger' mode was used to accumulate statistics for probability measurements using pion and proton beams of various intensities. Additionally, a 'trigger burst' mode was used with a pion beam so that the recovery of the chip following a HIP event could be studied. Each trigger burst was initiated by a particle trigger provided by the upstream counter and comprised ten triggers issued to the readout system, with consecutive triggers spaced by 75 ns. The APV25 chips were operated in 'multi-mode', providing peak-sampled data from three consecutive 25 ns time intervals for each trigger received. Hence, this 'trigger burst' mode provided data from the readout system every 25 ns over a 750 ns time interval.

5.2. The X5 beam test

Complementary measurements were carried out during a further beam test at the CERN X5 beamline. The experimental set-up and measurement program were similar to those at PSI; only the important differences are outlined here. The X5 beamline provided a bunched 120 GeV/c pion beam at the LHC bunch crossing frequency of 40 MHz and an intensity of 2 MHz cm^{-2}. The tracking unit comprised five TOB modules, again equipped with both inverter resistor values. Importantly, the APV25 chips were operated in the nominal deconvolution mode, as well as peak mode (as at PSI) and inverting or non-inverting mode. Statistics were accumulated during 'trigger burst' runs, providing useful data describing the temporal behaviour of the APV25 chip when operated in deconvolution mode. Data were also collected during 'single trigger' runs. However, the 'HIP event' probability study was complicated by the fact that, unlike at PSI, no trigger pre-filter was used and the presence of significant detector material upstream of the TOB tracking unit, acting as a pre-shower, affected the beam purity in terms of both particle composition and momentum.

6. Beam test measurements of the HIP event probability

HIP events are identified on the basis of their effect on the APV25 pulse height data. Large, negative CM levels are used to identify HIP events and the presence of a substantial signal (typically $\gtrsim$4 MIPs) is also required to ensure that the CM offset is due to a large energy release in the sensor. The integral HIP event probability, P_{hip}, is obtained from a given data sample by normalising the number of HIP events, N_{hip}, that induce a CM level below the threshold $\mathrm{CM}_{\mathrm{cut}}$ to the total number of particles incident on a single sensor plane, N_{track}, such that

$$P_{\mathrm{hip}}(\mathrm{CM}_{\mathrm{cut}}) = N_{\mathrm{hip}}(\mathrm{CM} < \mathrm{CM}_{\mathrm{cut}})/N_{\mathrm{track}}.$$

The total number of incident particles, N_{track}, is defined by the product of the number of triggered events and the mean particle multiplicity per sensor plane (0.7–1.5), which is observed to depend on both the beam configuration and trigger conditions. Alternatively, the CM level can be expressed in terms of the absolute CM level normalised to the minimum possible CM level ($\mathrm{CM}_{\mathrm{min}}$) that is dependent on the APV25 bias settings [8]. Hence, a 'CM ratio' (CMR) value of 0 corresponds to pulse height data at their nominal pedestal levels and -1 corresponds to pulse height data fully depressed to the lower limit of the APV25 dynamic range. The integral HIP event probability is, in this case, expressed as a function of the threshold $\mathrm{CMR}_{\mathrm{cut}}$.

6.1. Probability measurements with 300 MeV/c pions

Fig. 7 shows the integral HIP event probability curves as a function of $\mathrm{CMR}_{\mathrm{cut}}$ measured for different module configurations with the 'high' intensity π^- beam. The module configurations are

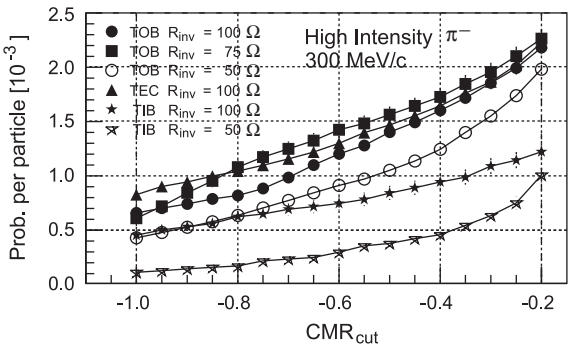

Fig. 7. Integral HIP event probability (per particle per sensor plane) as a function of CMR_{cut} for a high-intensity π^- beam and the various module configurations. The APV25 chips are operated in peak and inverting modes. Error bars represent statistical errors.

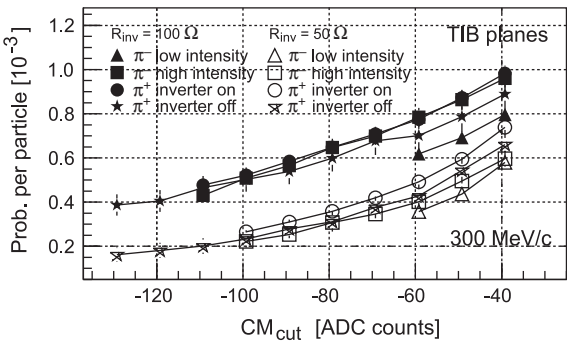

Fig. 8. Integral HIP event probability (per particle per sensor plane) as a function of CM_{cut} measured for TIB modules and various beam configurations. The APV25 chips are operated in various modes. Error bars represent statistical errors.

grouped according to module type (TIB, TEC and TOB) and inverter resistor value (50, 75 and 100 Ω). The integral curves provide the probability per incident pion per sensor plane of observing a CMR value below the threshold CMR_{cut}. As expected, the probability scales with the sensor thickness when considering modules equipped with the same inverter resistor value by the ratio $P_{hip}^{TIB}/P_{hip}^{TOB} \approx 320/500$. The measured probabilities for observing fully depressed baselines ($CMR_{cut} = -1$) are $<10^{-3}$ (per pion per sensor plane) for all module configurations.

Fig. 8 shows the integral HIP event probability curves as a function of CM_{cut} measured for TIB modules equipped with resistors of 100 and 50 Ω and for four different run configurations. The left-hand end-points of the individual curves represent the minimum observable CM level (CM_{min}). The curves show that the HIP event probability is independent of pion charge (which simply reflects the comparable inelastic cross-sections), beam intensity (as expected) and the APV25 inverter operating mode (inverter stage switched in or out). Also, a reduction of the HIP event probability is observed for modules equipped with the lower resistor value.[5]

[5]By definition, the 'HIP event' probability, P_{hip}, is dependent on both the cross-section for high-energy releases and the response of the APV25 chip to these energy releases.

Table 4
HIP event probability measurements, P_{hip}, for various thresholds with a high intensity 300 MeV/c π^- beam and the various module configurations

Module type	R_{inv} (Ω)	P_{hip} (10^{-4} per particle per sensor plane)		
		$CM_{cut}(-40)$	$CM_{cut}(-90)$	$CMR_{cut}(-0.8)$
TIB	50	6.0 ± 0.4	2.5 ± 0.2	1.7 ± 0.3
TIB	100	9.6 ± 0.5	5.6 ± 0.4	6.2 ± 0.6
TEC	100	17.3 ± 0.3	9.9 ± 0.3	10.4 ± 0.4
TOB	50	15.3 ± 0.3	7.9 ± 0.2	6.4 ± 0.3
TOB	75	19.6 ± 0.6	10.5 ± 0.4	10.8 ± 0.6
TOB	100	18.2 ± 0.4	9.8 ± 0.3	8.2 ± 0.4

The APV25 chips are operated in peak and inverting modes. The errors reported are statistical.

Table 4 details the HIP event probability measurements for various CM_{cut} and CMR_{cut} values. The measurements for $CM_{cut} = -90$ ADC counts can be (approximately) compared with those for $CMR_{cut} = -0.8$. Each measurement corresponds to the mean value for a category of module configuration and the quoted uncertainties represent the statistical error. The probability measurements obtained from modules of the same type, equipped with the same resistor value and for the same beam configuration, match to better than 15%. The mean ratio of the probability measurements, averaged over the entire CM_{cut} range, for identical modules equipped with different inverter

resistor values is $P_{\mathrm{hip}}^{50\,\Omega}/P_{\mathrm{hip}}^{100\,\Omega} = 0.80 \pm 0.16$ for the TOB modules and 0.59 ± 0.10 for the TIB modules.

The main systematic uncertainty is in the determination of the normalisation factor N_{track}. Pile-up, back-scattered pions and particle production through interactions in the sensors or support structures all contribute to the mean pion multiplicity. The probability measurements are therefore inclusive of all effects induced by pion interactions on the 12 detector planes exposed to the beam; comparing the measurements from the same modules for different runs yields a variation of ±15%. The uncertainty associated with the threshold on the HIP signal magnitude is negligible due to the removal of 'HIP event' pile-up by the trigger pre-filter. Furthermore, two independent analyses have been performed, which use different methods to zero-suppress the data and reconstruct clusters; the results of the two analyses are in agreement to better than 10%.

6.2. Probability measurements with 120 GeV/c pions

Fig. 9 plots the integral HIP event probability curves as a function of $\mathrm{CM_{cut}}$ for TOB modules illuminated by a 120 GeV/c pion beam. Curves are shown for modules equipped with 120 or 50 Ω resistors and for APV25 chips operated in deconvolution and inverting mode, deconvolution and non-inverting mode, and peak and non-inverting mode. Table 5 summarises the HIP event probability measurements performed with the APV25 chips operating in the above configurations. The measurements are comparable to those performed at PSI, with no significant differences observed between operating in peak and deconvolution modes and inverting and non-inverting modes. No decrease in the 'HIP event' probability is observed for the reduced inverter resistor value.

With respect to the PSI measurements, two additional sources of uncertainty are present in the X5 measurements. As previously mentioned, the presence of the material upstream of the tracking system acts as a pre-shower, creating high-multiplicity events that are likely to contain low-momentum pions (and other particles) with non-normal angles of incidence. These particles have an increased probablity of releasing a significant amount of energy in a sensor plane and so can bias the probability measurement. Employing a software-based filter that removes events containing high particle multiplicities in the first and second sensor planes from the data sample results

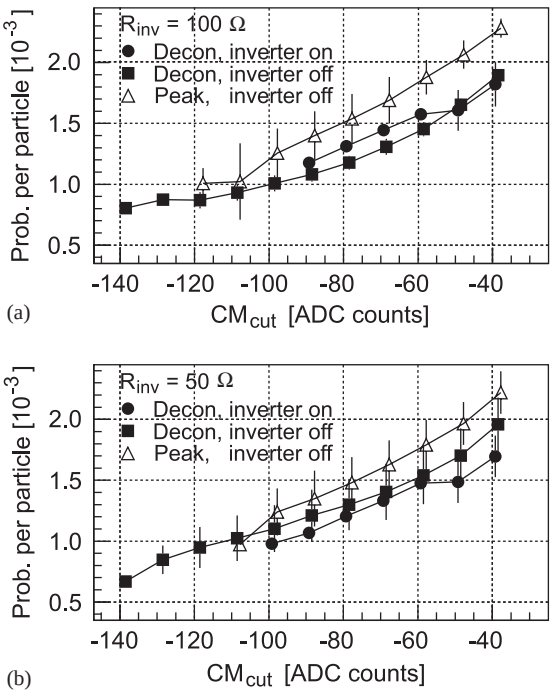

Fig. 9. Integral HIP event probability (per particle per sensor plane) as a function of $\mathrm{CM_{cut}}$ measured for TOB modules, with a 120 GeV π^- beam and two different resistor values. The APV25 chips are operated in various modes. The mean probability is plotted for the relevant module configuration; the error bars represent the error on the mean probability.

Table 5
HIP event probability measurements, P_{hip}, for various thresholds with a 120 GeV π^- beam and two inverter resistor values

Module type	R_{inv} (Ω)	P_{hip} (10^{-4} per particle per sensor plane)		
		$\mathrm{CM_{cut}}(-40)$	$\mathrm{CM_{cut}}(-90)$	$\mathrm{CMR_{cut}}(-0.8)$
TOB	50	16.7 ± 0.4	10.7 ± 0.4	9.3 ± 0.3
TOB	100	14.3 ± 0.3	10.4 ± 0.4	10.5 ± 0.2

The APV25 chips are operated in deconvolution and inverting modes. The errors reported are statistical.

in probability measurements that are 30–40% lower. Additionally, as no trigger pre-filter was used in this beam test, the presence of HIP event 'pile-up' is non-negligible, especially when operating in inverting mode due to the persistence of the HIP-induced signal over several hundred ns (this is not the case for non-inverting mode). Varying the threshold on the HIP signal magnitude between 0 to 200 ADC counts changes the probability measurements by ±20%.

6.3. Comparison of probability measurements with simulation

The behaviour of the APV25 baseline in response to large signals, as described in Section 3, can be used to relate the observed CM shifts in the APV25 data to the energy deposition magnitudes. The data collected at PSI with the 300 MeV/c proton beam reveals a peak in the CM distribution centered on CM ≈ -15 ADC counts. The Bethe–Bloch equation [12] predicts that 300 MeV/c protons will release a mean energy of 1 MeV in 500 μm silicon. Assuming a linear relationship [5,9], a CM level of -90 ADC counts therefore corresponds to an energy deposition of ~ 6 MeV. The probability of observing an energy deposition of at least 6 MeV, as provided by Fig. 3, is $\sim 10^{-3}$, which is in excellent agreement with the experimental measurements of $P_{\mathrm{hip}}\ (\mathrm{CM} = -90) = (7.9 - 10.5) \times 10^{-4}$ for the TOB modules. Similarly, the predicted probability of 14×10^{-4} for energy depositions of at least 3 MeV compares well with the experimental measurements of $P_{\mathrm{hip}}\ (\mathrm{CM} = -40) = (15.3 - 19.6) \times 10^{-4}$, again for TOB modules.

The laboratory studies show that an energy threshold of ~ 10 MeV is required in order to induce significant deadtime in the chip. This is comparable to the 6–9 MeV energy deposition required to depress the CM level to -90 to -120 ADC counts, which is typical for fully depressed baselines. Additionally, since the maximum energy deposition generated by elastic collisions is 3 MeV (as shown in Fig. 2), it can be expected that elastic collisions rarely induce deadtime in the APV25. This is indirectly confirmed by the HIP event probability measurements performed with a muon beam [1].

7. Recovery of the APV25 baseline following a HIP event

Figs. 10(a) and (b) show how the APV25 'baseline' pulse height data recover with time, in terms of the CMR variable, following HIP events that initially fully depress the baseline. The APV25s were operated in deconvolution mode (with readout every 75 ns) and the modules were equipped with resistor values of 100 and 50 Ω. The plots clearly show that the baseline can remain fully depressed (CMR $= -1$) for up to 300 ns and there is frequently an overshoot during the recovery period. When the APV25 is operated in peak mode, the baseline is observed to remain fully depressed for up to 200 ns. The laboratory measurements suggest that the period for which the baseline remains fully depressed is indicative of the deadtime experienced by the chip.

Additionally, during the recovery of an APV25 chip affected by a HIP event, the analogue data levels are frequently non-uniform across the 128 channels, as illustrated by the data shown in Fig. 1. This is potentially a serious problem, since zero suppression of the data (which involves CM level

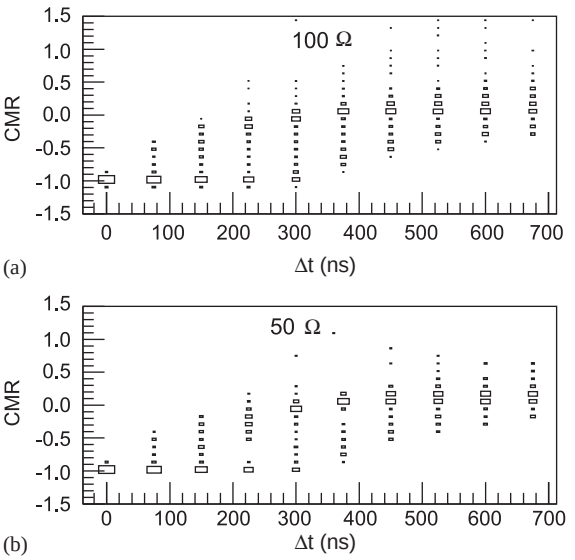

Fig. 10. Time evolution of APV25 recovery following a HIP event, expressed in terms of the CMR variable. The APV25 chips are operated in deconvolution and inverting modes and are equipped with resistor values of (a) 100 Ω or (b) 50 Ω.

subtraction) will be performed by an off-detector VME board [13]. Currently, it is envisaged that the CM level will be estimated from the median value of the 128 pulse height data provided by each chip, which implicitly assumes a uniform shift in the data of all channels. Hence, non-flat baselines may lead to the zero-suppression algorithm rejecting channels with genuine signals (generating inefficiencies) or identifying extra 'fake' hits in channels that do not actually have a genuine signal (increasing the data rate).

The default zero-suppression algorithm passes isolated channels ('strips') with signal-to-noise ratios of $(S/N)\geqslant 5$ and groups of two or more non-isolated strips with $(S/N)\geqslant 2$ (however, these thresholds are programmable). Fig. 11 plots the mean number of fake strips per APV25 accepted by the algorithm. To isolate the contribution due to baseline distortions, the number plotted is the difference between that obtained from chips affected by HIP events and that from chips operating under normal conditions. The plot is based on X5 data taken in deconvolution and inverting mode. The number of fake strips is significantly increased for a resistor value of 50 Ω.

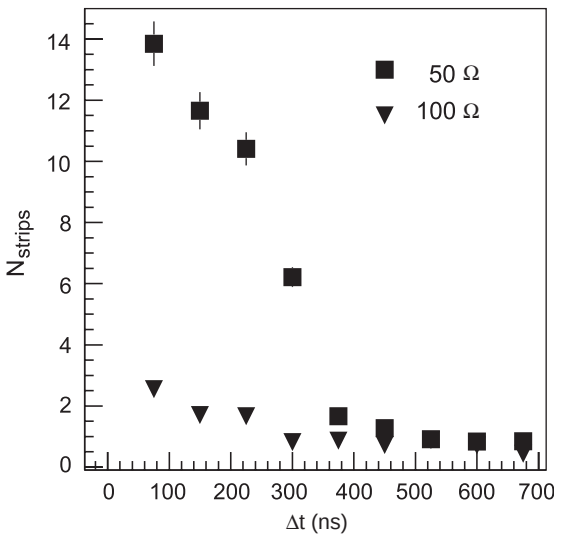

Fig. 11. Mean number of fake strips per APV25 due to baseline distortions, as a function of time elapsed since the HIP event for modules equipped with resistors of $R_{inv} = 100\,\Omega$ (triangles) or 50 Ω (squares).

Table 6
Mean number of fake strips and the expected (absolute) increase in strip occupancy in the innermost CMS tracker layer due to non-flat baselines caused by HIP events for various APV25 operating modes and resistor values

Mode	R_{inv} (Ω)	N_{strip}	Δ_{occ} (%)
Decon	50	143 ± 8	0.14 ± 0.01
Decon	100	31 ± 2	0.04 ± 0.00
Peak	50	290 ± 11	0.29 ± 0.01
Peak	100	230 ± 10	0.31 ± 0.02

In the innermost layer of the SST, the expected strip occupancy in high-luminosity proton–proton LHC running is 2.8%. Fake strips due to HIP events will increase this occupancy by

$$\Delta_{occ} = (N_{strip}/128) \times \overline{P_{hip}}$$

where N_{strip} is the expected total number of fake strips generated by a HIP event and $\overline{P_{hip}}$ is the mean probability per APV25 chip for a HIP event to occur in a given bunch crossing. For the innermost sensor layer, where the occupancy is highest, $\overline{P_{hip}}$ is expected to be 17×10^{-4} (13×10^{-4}) for $R_{inv} = 100\,\Omega$ (50 Ω), as reported in Section 9. The value of N_{strip} is calculated by summing over all time bins shown in Fig. 11 (and multiplying by three for the X5 data to account for the 75 ns readout period). Table 6 shows the predicted occupancy increase for various module configurations. The increase is small when compared with the total occupancy, particularly for APV25 chips operating in deconvolution mode, which is the nominal mode of operation.

8. Beam test measurements of the HIP-induced inefficiency

The efficiency of the APV25 during the recovery period following a HIP event can be measured by searching for signals associated with the passage of a reconstructed MIP track. The special 'trigger burst' data acquisition mode allows the cluster reconstruction efficiency to be calculated throughout a 750 ns temporal window. Sufficient statistics for this analysis were only collected during the PSI beam test when the APV25 chip was operated in

peak and inverting mode. The selection criteria used to identify HIP events are identical to those described in Section 6. The sample of HIP events is defined using a loose threshold, $CM_{thr} = -40$ ADC counts, so that the results are inclusive of all contributions to the induced inefficiencies. Clusters are reconstructed from zero-suppressed data using an algorithm comparable to those detailed in Ref. [15]. All combinations of MIP-induced clusters, excluding those found in the sensor plane affected by a HIP event, are fitted to a straight line track. Tracks with a sufficiently good fit and transversing all six TOB sensor planes (the TIB and TEC planes are not used in this analysis) are selected and extrapolated to the module affected by the HIP event, where they intercept part of the sensor instrumented by either an affected or unaffected APV25 chip. The presence of a reconstructed cluster within a narrow search window around the intercept point signifies an 'efficient' APV25 chip.

The efficiency of both affected and unaffected APV25 chips is measured as a function of the time elapsed since the HIP event. The efficiency of the tracking algorithm under normal APV25 operating conditions is better than 98% and time-independent. The efficiencies exhibited by HIP-affected chips are normalised to those observed for unaffected chips in order to correct for the (small) inadequacies in the tracking algorithm and inefficiencies intrinsic to the readout system. Fig. 12 plots the measured efficiency as a function of time elapsed since the HIP event (100 ns bins) for HIP-affected chips equipped with the different resistor values. A clear improvement is seen in the case of the 50 Ω resistor. Figs. 13(a) and (b) plot the CM levels observed during the recovery period of 'efficient' and 'inefficient' chips, respectively, versus time elapsed since the HIP event (Δt); 'efficient' indicates that the signal is observed in the search window defined by a MIP track at time Δt. For the 'efficient' case, the CM levels are observed to return to nominal values within ~300 ns. For the inefficient case, the CM levels are typically fully depressed immediately after the HIP event and for up to 200 ns; these chips are observed to remain inefficient for up to 700 ns following a HIP event.

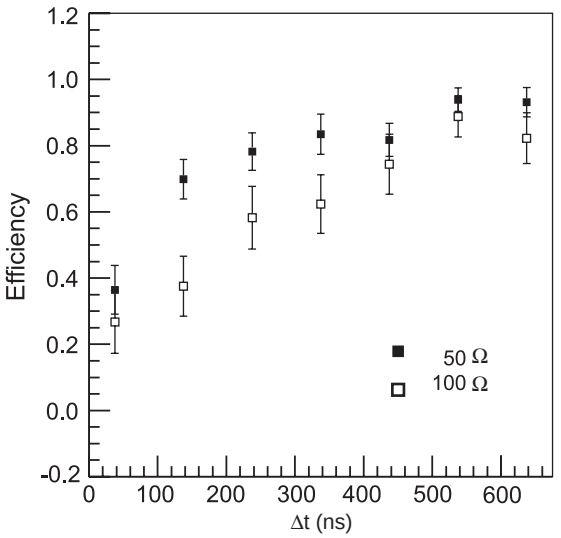

Fig. 12. Cluster reconstruction efficiency as a function of time elapsed since the HIP event for affected APV25 chips equipped with inverter resistors of 100 Ω (open markers) or 50 Ω (closed markers).

The average inefficiencies measured over the full 750 ns time window for various CM_{cut} thresholds and inverter resistor values are listed in Table 7; a change in resistor value from 100 to 50 Ω reduces the inefficiency by ~40%. In the HIP event sample selected by $CM_{cut} < -90$ ADC counts, which is likely to induce deadtime, the "effective deadtimes" (reflecting the averaged inefficiencies over the 750 ns time window) are 345 ± 23 ns (100 Ω) and 210 ± 15 ns (50 Ω), in fair agreement with the laboratory studies. The systematic uncertainty associated with the inefficiency measurements resulting from the choice of selection criteria, cluster and track-finding algorithms is estimated to be ±15%.

9. Expected effect on the CMS SST performance

The 'HIP event' interaction length, λ_{hip}, for pions in silicon is calculated by normalising the HIP event probability measurements for $CM_{cut} = -40$ ADC counts, listed in Table 4, to the mean path length of the incident pions in silicon. The tracking units at PSI and X5 were illuminated by

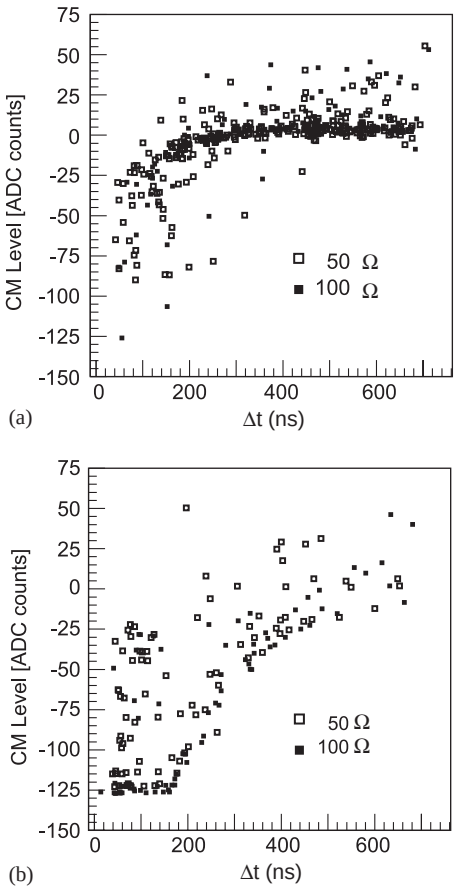

Fig. 13. CM level versus time for (a) 'efficient' and (b) 'inefficient' chips equipped with inverter resistors of 100 Ω (closed markers) or 50 Ω (open markers).

Table 7
Average APV25 inefficiency over the 750 ns time interval following a HIP

CM_{cut} (ADC counts)	R_{inv} (Ω)	η (%)
−40	100	36 ± 2
−40	50	21 ± 2
−90	100	46 ± 3
−90	50	28 ± 2

Results are shown for different inverter resistor and CM_{cut} values. The errors reported are statistical.

particles at normal incidence in the absence of a magnetic field, so the mean path length is considered to be the sensor thickness. Table 8 lists the measured values of λ_{hip} and their associated statistical uncertainties obtained for the TOB modules.

Table 8
Mean inelastic nuclear interaction length corresponding to the measured HIP event probability for $CM_{cut} = -40$ ADC counts for the two resistor values

R_{inv} (Ω)	λ_{hip} (cm)
100	28 ± 1
50	38 ± 2

Only statistical errors are shown.

As described in Section 6.3, a CM level of −40 ADC counts corresponds to an energy release of 3 MeV, which is comparable to the minimum energy release induced by inelastic nuclear collisions. The corresponding integral probability (14×10^{-4}, as provided by Fig. 2) is equivalent to an interaction length of 35 cm, which is in good agreement with the values quoted in Table 8 and, as expected, comparable to the nuclear interaction length in silicon, i.e. 45 cm at high energies [14].

When extrapolating the beam test results to the CMS SST environment, the dependence of λ_{hip} on the particle type and energy spectra must be accounted for. As shown in Fig. 3, neglecting the dependence on the particle type and momentum introduces about 50% additional uncertainty with respect to the curve obtained for mono-energetic pions. More important could be the effects of very-low-momentum tracks, which can release several MeV by ionisation alone, as was observed with the proton beam during the PSI beam test. The effects of these 'ionisation HIPs' are not included in the interaction length λ_{hip} measured with the pion beam, as the pion momentum was too high to cause such effects. Studies of simulated minimum bias events in the CMS tracker show that only protons will release more than 10 MeV through ionisation, with a probability that is about 10 times larger than releasing this energy through a nuclear interaction. Below 10 MeV, the laboratory measurements of Section 4 show that no significant inefficiency is produced in the APV25. Thus, 'ionisation HIPs' are accounted for by applying a factor 10 to the expected mean proton path length in silicon in the SST.

Table 9
Mean weighted path length, $\overline{D}$ (μm), of hadrons in silicon per APV25 chip per bunch crossing for the first and last microstrip detector layers (at radius R) in the SST barrel region, as obtained from CMSIM/ORCA and FLUKA flux predictions

R (cm) (region)	22 (TIB)	115 (TOB)
CMSIM/ORCA	480	100
FLUKA	355	57.5

Table 10
Predicted inefficiencies in the first TIB tracking layer (at a radius of 22 cm) for the two inverter resistor values

R_{inv} (Ω)	$\overline{\eta}$ (%)
100	1.9 ± 0.2
50	0.8 ± 0.1

Only statistical errors are shown.

Table 11
Hit inefficiencies due to HIP events for isolated muon tracks and tracks belonging to b-jets with 100 GeV transverse energy

Layer	No HIP events	With HIP events	
	Isolated muons	Isolated muons	b-jets
1	0.004 ± 0.001	0.013 ± 0.002	0.020 ± 0.002
3	0.003 ± 0.001	0.009 ± 0.002	0.019 ± 0.002
5	0.002 ± 0.001	0.014 ± 0.001	0.022 ± 0.002
9	0.001 ± 0.001	0.002 ± 0.001	0.007 ± 0.002

The first column quotes the (intrinsic) inefficiencies observed when the HIP effect is not simulated. All predicted inefficiencies are for modules equipped with 50 Ω resistors.

At the LHC, each signal event is superimposed over a number of minimum bias events. These minimum bias events consist mostly of low-energy pions, which are confined by the 4 T magnetic field to the inner part of the SST. In both high- and low-luminosity operation, the majority of the interactions between particles and silicon sensors is due to these minimum bias events, and only in the narrow regions inside hadronic jets do the signal events contribute significantly to the hit density. The average probability per APV25 chip for a HIP event to occur in a given LHC bunch-crossing is given by

$$\overline{P_{\mathrm{hip}}} = \overline{D}/\lambda_{\mathrm{hip}}$$

where $\overline{D}$ is the mean total path length (summed over all particle types) per APV25 chip per bunch crossing due to minimum bias event pile-up. Table 9 shows values for $\overline{D}$ in the innermost and outermost barrel layers, as provided by a simulation of high-luminosity running conditions using CMSIM/ORCA [15]. The results have been cross-checked against the values listed in Table 1 that are provided by a FLUKA simulation. As the FLUKA predictions are found to be lower, results from CMSIM/ORCA are used to be conservative.

9.1. Hit reconstruction inefficiencies

As shown in Section 8, an APV25 can remain inefficient for several bunch crossings following a HIP event, although a complete recovery is almost achieved within 750 ns (30 bunch crossings). Therefore, the efficiency loss due to HIP events occurring in minimum bias events is

$$\overline{\eta} = 30 \times \overline{P_{\mathrm{hip}}} \times \eta$$

where η is the average inefficiency in the 30 bunch crossings following a HIP event, as reported in Table 7. For an isolated muon inside the SST, hits are lost only due to minimum bias events since the probability of an HIP due to the muon itself is negligible. In Table 10, the expected hit inefficiency in the first TIB layer is shown for two different resistor values. The ratio of inefficiencies observed with the resistor value 100 Ω with respect to 50 Ω is $2.4 \pm 0.4 \pm 0.7$, where the uncertainties are statistical and systematic, respectively. The systematic uncertainty is dominated by the uncertainty in the ratio of the interaction lengths.

To study the effect of 'dense' hadronic signal events, the APV25 inefficiency due to HIP events has been implemented in the simulation. The expected hit inefficiencies for modules equipped with 50 Ω resistor are shown in Table 11 for isolated muons and for tracks belonging to b-jets with a transverse energy of 100 GeV. These inefficiencies would approximately double with a 100 Ω resistor.

9.2. Tracking performances

Tracking efficiencies and resolutions are not significantly affected by HIP events. On average, a track results from a fit to more than 11 points; losing one hit does not result in the track being 'lost' or affect the resolution of the track parameters [15]. Furthermore, since during reconstruction a track is only lost if two consecutive hits are missing, the expected tracking inefficiency due to HIPs is only $\approx 10 \times \overline{\eta}^2$. Therefore, using the hit inefficiencies provided by Table 11, one expects a track inefficiency of only 0.2% for single muons and 0.4% for b-jet tracks with a 50 Ω resistor. If a 100 Ω resistor were used, the inefficiency would reach 2% in b-jets. These values were verified by running the standard CMS track reconstruction algorithms on events generated by the CMSIM/ORCA simulation. Even for very conservative estimates of the hit inefficiencies, there is minimal effect on track reconstruction efficiency and b-tagging performance [5].

10. Summary

Highly ionising particles (HIPs) produced by inelastic nuclear interactions in the CMS silicon strip tracker sensors are observed to produce large signals that can momentarily saturate the APV25 readout chip. Studies of these 'HIP events' in the laboratory highlight the sensitivity of the effect on the value of a resistor used in the power supply line to the APV25 inverter stage. Reducing this resistor value significantly moderates the effect of HIP events on the APV25 chip and, as a consequence, modules of the SST readout system will be equipped with a reduced resistor value of 50 Ω.

Detailed studies of the HIP effect have also been performed using beam test data accumulated at PSI and the CERN X5 beamline. The probability of a 300 MeV/c pion (the most probable pion momentum expected in the CMS SST) inducing a HIP event when transversing 320-μm-thick sensors has been measured to be in the range $(3-10) \times 10^{-4}$, depending on the severity of the HIP event. As expected, the probability is observed to scale with the sensor thickness. The measured probabilities are found to be in excellent agreement with Monte Carlo simulations of this effect.

Large HIP signals act to depress the APV25 pulse height data. The temporal evolution of the data levels is studied using a special 'trigger burst' operating mode, which provides data from 30 consecutive (25 ns) bunch-crossing periods. The levels are observed to recover over a period of a few hundred nano-seconds and no significant dependence of the recovery time on sensor thickness is seen. However, the levels recover about 20% faster with the reduced resistor value of 50 Ω. During the recovery, the pulse height data are typically not flat across the 128 channels and frequently exhibit large distortions. An off-detector ADC and processing board will perform zero-suppression of the APV25 pulse height data, which involves CM subtraction. Presently, the CM algorithm assumes uniform flat data and, as a consequence, wide 'fake' clusters are generated. However, under normal CMS running conditions, the low HIP event rate means that these are expected to increase the strip occupancy by only one part in twenty if the reduced resistor value (50 Ω) is used, and virtually nothing for the nominal 100 Ω case.

The efficiency of the APV25 chip following a HIP event is investigated by reconstructing MIP tracks and using these tracks to search for signal within the pulse height data of chips affected by HIP events. Large inefficiencies are measured at the time of a HIP event and a recovery in the efficiency is observed over the subsequent few hundred nano-seconds. The mean inefficiency measured over a 750 ns time window is $36 \pm 2\%$ ($21 \pm 2\%$) for a resistor value of 100 Ω (50 Ω). These inefficiencies are consistent with deadtime measurements obtained from laboratory studies of the effect.

The HIP event probability measurements and the mean inefficiency induced by HIP events have been combined with Monte Carlo estimates of particle fluxes at CMS to predict the total inefficiency due to the HIP effect in the CMS SST. In the innermost barrel layer, where the effect is expected to be the most severe, the hit inefficiency is $1.9 \pm 0.2\%$ ($0.8 \pm 0.1\%$) for an inverter resistor value of 100 Ω (50 Ω). The simulations also show

that the effect is expected to minimal effect on the track reconstruction efficiency and the *b*-tagging performance of the SST.

Acknowledgements

We thank the hospitality of the Paul Scherrer Institut, Villigen, Switzerland, where much of this work was performed. We also thank L. Berretta for his help in building the mechanics of the supporting boxes, C. Girerd for his precious help with the TSC modules and J. Martin and J. Hill for their help during the PSI setup installation.

References

[1] R. Bainbridge, et al., The effect of highly ionising events on the APV25 readout chip, CMS Note 2002-038.
[2] M.J. French, et al., Nucl. Instr. and Meth. A 466 (2001) 359.
[3] The CMS Tracker Collaboration, The tracker project: technical design report, CERN/LHCC 1998-006; The tracker project: TDR addendum, CERN/LHCC 2000-016.
[4] The CMS Collaboration, The compact muon solenoid: technical proposal, CERN/LHCC 1994-038.
[5] W. Adams, et al., Test-beam analysis of the effect of highly ionising particles on the silicon strip tracker, CMS Note 2003-025.
[6] M. Huhtinen, Highly ionising events in silicon detectors, CMS Note 2002-011.
[7] M. Huhtinen, F. Faccio, Nucl. Instr. and Meth. A 450 (2000) 155.
[8] L.L. Jones, et al., The APV25 deep submicron readout chip for CMS detectors, CERN/LHCC 1999-033.
[9] R. Bainbridge, Influence of highly ionising events on the CMS APV25 readout chip, Doctoral Thesis for the University of London, June 2004, CERN-THESIS-2004-032.
[10] Meta-Software, HSPICE User's Manual, Version 96.1, February 1996.
[11] L. Mirabito, et al., Response of the APV readout chip to laser-simulated, highly ionizing interactions, CMS Note 2004-022.
[12] S. Eidelman, et al., Phys. Lett. B 592 (2004) 1 (Sec. 27). http://pdg.lbl.gov.
[13] J. Coughlan, et al., The front-end driver card for the CMS silicon strip tracker readout, CERN/LHCC/2002/034, 296.
[14] S. Eidelman, et al., Phys. Lett. B 592 (2004) 1 (Sec. 6). http://pdg.lbl.gov.
[15] The CMS Collaboration, The TriDAS Project TDR: data acquisition and higher level trigger, CERN/LHCC 2002-026 (Chapter 14).